References

Akal, T., and J. Hovem (1978), Two-dimensional space series analysis for sea-floor roughness, *Marine Geotechnology*, *3*(2), 171–182.

Amos, C., A. Bowen, D. Huntley, and C. Lewis (1988), Ripple generation under the combined influences of waves and currents on the Canadian continental shelf, *Continental Shelf Research*, *8*(10), 1129–1153.

Ardhuin, F., T. Herbers, and W. O'Reilly (2001), A hybrid eulerian-lagrangian model for spectral wave evolution with application to bottom friction on the continental shelf, *Journal of Physical Oceanography*, *31*(6), 1498–1516.

Ardhuin, F., T. Drake, and T. Herbers (2002), Observations of wave-generated vortex ripples on the North Carolina continental shelf, *Journal of Geophysical Research*, *107*(C10), 3143, doi:10.1029/2001JC000986.

Ashida, K., and Y. Tanaka (1967), Experimental study on sand waves, *Disaster Prevention Research Institute Annuals, Kyoto University*, *10*, 121–132.

Ayrton, H. (1911), The origin and growth of ripple-mark, *Proceeding of the Royal Society of London*, *84*(A), 285–310.

Baas, J. (1994), A flume study on the development and equilibrium morphology of current ripples in very fine sand, *Sedimentology*, *41*, 185–209.

Baas, J. (1999), An empirical model for the development and equilibrium morphology of current ripples in fine sand, *Sedimentology*, *46*, 123–138.

Bagnold, R. (1946), Motion of waves in shallow water, *Proceedings Royal Society London Series A*, *187*, 1–15.

Bell, P., and P. Thorne (1997), Measurements of sea bed ripple evolution in an estuarine environment using a high resolution acoustic sand ripple profiling system, in *Oceans '97*, pp. 815–819, IEEE, Halifax.

Bell, T. (1975), Statistical features of sea-floor topography, *Deep-Sea Research*, *22*, 883–892.

Beresford, P. (1998), HR wavemaker wave generation control program: software manual, *Tech. Rep. IT 453*, HR Wallingford Ltd.

Betteridge, K., J. Williams, P. Thorne, and P. Bell (2003), Acoustic instrumentation for measuring near-bed sediment processes and hydrodynamics, *Journal of Experimental Marine Biology and Ecology*, *285-286*, 105–118.

Blondeaux, P. (2001), Mechanics of coastal forms, *Annual Review of Fluid Mechanics*, *33*, 339–370.

Booij, N., R. Ris, and L. Holthuijsen (1999), A third-generation wave model for coastal regions, 1. model description and validation, *Journal of Geophysical Research*, *104*(C4), 7649–7666.

Briggs, K. (1989), Microtopographical roughness of shallow-water continental shelves, *IEEE Journal of Oceanic Engineering*, *14*(4), 360–367.

Briggs, K., D. Tang, and K. Williams (2002), Characterization of interface roughness of rippled sand off Fort Walton beach, Florida, *IEEE Journal of Oceanic Engineering*, *27*(3), 505–514.

Carstens, M., R. Neilson, and H. Altinbilek (1969), Bed forms generated in the laboratory under oscillatory flow: Analytical and experimental study, *Tech. Memo. 28*, US Army Corps of Eng. Coastal Eng. Res. Center.

Clifton, H. (1976), Wave-formed sedimentary structures: A conceptual model, in *Beach and Nearshore Sedimentation, SEPM Special Publication*, vol. 27, edited by R. Davis and L. Ethington, pp. 327–342.

Clifton, H., and J. Dingler (1984), Wave-formed structures and paleoenvironmental reconstruction, *Marine Geology*, *60*, 165–198.

Coleman, S., and B. Melville (1996), Initiation of bed forms on a flat sand bed, *Journal of Hydraulic Engineering ASCE*, *122*(6), 301–310.

Crawford, A., and A. Hay (1998), A simple system for laser-illuminated video imaging of sediment suspension and bed topography, *IEEE Journal of Oceanic Engineering*, *23*(1), 12–19.

Crawford, A., and A. Hay (2001), Linear transition ripple migration and wave orbital velocity skewness: Observations, *Journal of Geophysical Research*, *106*(C7), 14,113–14,128.

Dade, W., A. Hogg, and B. Boudreau (2001), Physics of flow above the sediment-water interface, in *The Benthic Boundary Layer*, edited by B. Boudreau and B. Jorgensen, pp. 4–43, Oxford Univ. Press, New York.

Doucette, J. (2002), Bedform migration and sediment dynamics in the nearshore of a low-energy sand beach in southwest Australia, *Journal of Coastal Research*, *18*(3), 576–591.

Drake, D., and D. Cacchione (1986), Field observations of bed shear stress and sediment resuspension on continental shelves, Alaska and California, *Continental Shelf Research*, *6*(3), 415–429.

Drake, D., and D. Cacchione (1989), Estimates of the suspended sediment reference concentration (C_a) and resuspension coefficient (γ_o) from near-bottom observations on the California shelf, *Continental Shelf Research*, *9*(1), 51–64.

Drake, D., and D. Cacchione (1992), Wave-current interaction in the bottom boundary layer during storm and non-storm conditions: observations and model predictions, *Continental Shelf Research*, *12*(12), 1331–1352.

Engelund, F., and J. Fredsoe (1982), Sediment ripples and dunes, *Annual Review of Fluid Mechanics*, *14*, 13–37.

Faraci, C., and E. Foti (2002), Geometry, migration and evolution of small-scale bedforms generated by regular and irregular waves, *Coastal Engineering*, *47*, 35–52.

Fox, C., and D. Hayes (1985), Quantitative methods for analyzing the roughness of the seafloor, *Reviews of Geophysical*, *23*, 1–48.

Fredsoe, J., K. Andersen, and B. Sumer (1999), Wave plus current over a ripple-covered bed, *Coastal Engineering*, *38*(4), 177–221.

Fukuoka, S. (1968), Generation, development and spectrum of sand waves, *Tech. rep.*, Department of Civil Engineering, Tokyo Institute of Technology.

Goda, Y. (1978), The observed joint distribution of periods and heights of sea waves, in *16th International Coastal Engineering Conference*, vol. 1, pp. 227–246, ASCE, Sydney, Australia.

Goda, Y. (2000), *Random seas and design of maritime structures*, *Advanced Series on Ocean Engineering*, vol. 15, 2nd ed., World Scientific.

Graber, H., and O. Madsen (1988), A finite-depth wind-wave model, part 1: model description, *Journal of Physical Oceanography*, *18*(11), 1465–1483.

Grant, W., and O. Madsen (1982), Movable bed roughness in unsteady oscillatory flow, *Journal of Geophysical Research*, *87*(C1), 469–481.

Grant, W., and O. Madsen (1986), The continental-shelf bottom boundary layer, *Annual Review Fluid Mechanics*, *18*, 265–305.

Grinvald, D., and V. Nikora (1988), *River Turbulence*, Hydrometeoizdat, Leningrad Russia (in Russian).

Hanes, D., V. Alymov, and Y. Chang (2001), Wave-formed sand ripples at Duck, North Carolina, *Journal of Geophysical Research*, *106*(C10), 22,575–22,592.

Hasselmann, K., et al. (1973), Measurements of wind-wave growth and swell decay during the joint north sea wave project (JONSWAP), *Tech. rep.*, Deutschen Hydrographischen Institut.

Hay, A., and D. Wilson (1994), Rotary sidescan images of nearshore bedform evolution during a storm, *Marine Geology*, *119*, 57–65.

Hino, M. (1968), Equilibrium-range spectra of sand waves formed by flowing water, *Journal of Fluid Mechanics*, *34*(3), 565–573.

Huettel, M., and I. Webster (2001), Porewater flow in permeable sediments, in *The Benthic Boundary Layer*, edited by B. Boudreau and B. Jorgensen, pp. 144–179, Oxford Univ. Press, New York.

Jain, S., and J. Kennedy (1974), The spectral evolution of sedimentary bed forms, *Journal of Fluid Mechanics*, *63*(2), 301–314.

Jorgensen, B., and B. Boudreau (2001), Diagenesis and sediment-water exchange, in *The Benthic Boundary Layer*, edited by B. Boudreau and B. Jorgensen, pp. 211–244, Oxford Univ. Press, New York.

Li, M., L. Wright, and C. Amos (1996), Predicting ripple roughness and sand resuspension under combined flows in a shoreface environment, *Marine Geology*, *130*, 139–161.

Lofquist, K. (1978), Sand ripple growth in a oscillatory-flow water tunnel, *Tech. Pap. 78-5*, US Army Corps of Eng. Coastal Eng. Res. Center.

Longuet-Higgins, F. (1983), On the joint distribution of wave periods and amplitudes in a random wave field, *Proceeding of the Royal Society of London*, *389*(A), 241–258.

Lyons, A., W. Fox, T. Hasiotis, and E. Pouliquen (2002), Characterization of the two-dimensional roughness of wave-rippled sea floors using digital photogrammetry, *IEEE Journal of Oceanic Engineering*, *27*(3), 515–524.

Madsen, O., P. Mathisen, and M. Rosengaus (1990), Movable bed friction factors for spectral waves, in *International Conference on Coastal Engineering Conference*, vol. 1, edited by B. L. Edge, pp. 420–429, ASCE, Delft.

Marsh, S., C. Vincent, and P. Osborne (1999), Bedforms in a laboratory wave flume: an evaluation of predictive models for bedform wavelengths, *Journal of Coastal Research*, *15*(3), 624–634.

Massel, S. (1996), *Ocean surface waves: their physics and prediction, Advanced series on Ocean Engineering*, vol. 11, World Scientific Publishing Co. Pty. Ltd., Singapore.

Mathisen, P., and O. Madsen (1999), Waves and currents over a fixed ripple bed 3. bottom and apparent roughness for spectral waves and currents, *Journal of Geophysical Research*, *104*(C8), 18,447–18,461.

Miller, M., and P. Komar (1980), A field investigation of the relationship between oscillation ripple spacing and the near-bottom water orbital motions, *Journal of Sedimentary Petrology*, *50*(1), 183–191.

Mogridge, G., and J. Kamphuis (1972), Experiments on bed form generation by wave action, in *Thirteenth Coastal Engineering Conference*, vol. 2, pp. 1123–1142, ASCE, Vancouver, Canada.

Mogridge, G., M. Davies, and D. Willis (1994), Geometry prediction for wave-generated bedforms, *Coastal Engineering*, *22*, 255–286.

Moore, K., and J. Jaffe (2002), Time-evolution of high-resolution topographic measurements of the sea floor using a 3-D laser line scan mapping system, *IEEE Journal of Oceanic Engineering*, *27*(3), 525–545.

Nielsen, P. (1981), Dynamics and geometry of wave-generated ripples, *Journal of Geophysical Research*, *86*(C7), 6467–6472.

Nielsen, P. (1992), *Coastal bottom boundary layers and sediment transport*, *Advanced series on Ocean Engineering*, vol. 4, World Scientific Publishing Co. Pty. Ltd., Singapore.

Nikora, V., and D. Hicks (1997), Scaling relationships for sand wave development in unidirectional flow, *Journal of Hydraulic Engineering*, *123*(12), 1152–1156.

Nordin, C. (1971), Statistical properties of dune profiles, *Geological Survey Professional Paper*, *562-F*, 448.

Nordin, C., and J. Algert (1966), Spectral analysis of sand waves, *Journal of the Hydraulic Division - ASCE*, *92*(HY5), 95–114.

O'Donoghue, T., and G. Clubb (2001), Sand ripples generated by regular oscillatory flow, *Coastal Engineering*, *44*, 101–115.

Phillips, O. (1958), The equilibrium range in the spectrum of wind-generated waves, *Journal of Fluid Mechanics*, *4*, 426–434.

Pierson, W., and L. Moskowitz (1964), A proposed spectral form for fully developed wind seas based on the similarity theory of S.A. Kitaigorodskii, *Journal of Geophysical Research*, *69*(24), 5181–5203.

Pouliquen, E., A. Lyons, and N. Pace (2000), Penetration of acoustic waves into rippled sandy seafloors, *Journal of the Acoustical Society of America*, *108*(5), 2071–2081.

Raudkivi, A. (1988), The roughness height under waves, *Journal of Hydraulic Research*, *26*(5), 569–584.

Ris, R., L. Holthuijsen, and N. Booij (1999), A third generation wave model for coastal regions 2. verification, *Journal of Geophysical Research*, *104*(C4), 7667–7681.

Shuliak, B. (1971), *Physics of waves on the surface of granular materials and fluids*, Nauka, Moscow, Russia (in Russian).

Sleath, J. (1984), *Sea Bed Mechanics*, Wiley Interscience, Cambridge University.

Soulsby, R. (1987), Calculating bottom orbital velocity beneath waves, *Coastal Engineering*, *11*(4), 371–380.

Swart, D. (1974), Offshore sediment transport and equilibrium beach profiles, *Tech. Rep. Pub. 131*, Delft Hydraulics Laboratory.

Toba (1973), Local balance in the air-sea boundary layer process, *Journal of Ocean Engineering Society Japan*, *29*, 209–220.

Tolman, H. (1994), Wind waves and moveable bed bottom friction, *Journal of Physical Oceanography*, *24*(5), 994–1009.

Tolman, H. (1995), Subgrid modelling of moveable-bed bottom friction in wind wave models, *Coastal Engineering*, *26*(1-2), 57–75.

Traykovski, P., E. Hay, A, J. Irish, and J. Lynch (1999), Geometry, migration, and evolution of wave orbital ripples at LEO-15, *Journal of Geophysical Research*, *104*(C1), 1505–1524.

Tsujimoto, T., and H. Nakagawa (1983), Sand wave formation due to irregular bed load motion, in *Mechanics of Sediment Transport proceedings of Euromech*, vol. 156, pp. 109–117.

Van Rijn, L. (1993), *Principles of sediment transport in rivers, estuaries and coastal seas*, Aqua Publications, Amsterdam.

Vincent, C., and P. Osborne (1993), Bedform dimensions and migration rates under shoaling and breaking waves, *Continental Shelf Research*, *13*(11), 1267–1280.

Vongvisessomjai, S. (1984), Oscillatory ripple geometry, *Journal of Hydraulic Engineering*, *110*(3), 247–266.

Wheatcroft, R. (1994), Temporal variation in bed configuration and one-dimensional bottom roughness at the mid-shelf stress site., *Continental Shelf Research*, *14*(10/11), 1167–1190.

Wiberg, P., and C. Harris (1994), Ripple geometry in wave-dominated environments, *Journal of Geophysical Research*, *99*(C1), 775–789.

Wiberg, P., and J. Smith (1985), A theoretical model for saltating grains in water, *Journal of Geophysical Research*, *90*(C4), 775–789.

Williams, J., P. Bell, P. Thorne, N. Metje, and L. Coates (2004), Measurement and prediction of wave generated suborbital ripples, *Journal of Geophysical Research*, *109*(C02004), doi:10.1029/203JC001882.

Willis, D., M. Davies, and G. Mogridge (1993), Laboratory observations of bedforms under directional irregular waves, *Canadian Journal of Civil Engineering*, *20*, 550–563.

Young, I. (1994), On the measurement of directional wave spectra, *Applied Ocean Research*, *16*, 283–294.

Young, I. (1995), The determination of confidence limits associated with estimates of the spectral peak frequency, *Ocean Engineering*, *22*(7), 669–689.

Young, I. (1999), *Wind generated ocean waves, Elsevier Ocean Engineering Book Series*, vol. 2, Elsevier, Oxford.

Young, I., and R. Gorman (1995), Measurements of the evolution of ocean wave spectra due to bottom friction, *Journal of Geophysical Research*, *100*(C6), 10,987–11,004.

Appendices

Appendix A

Conference Papers

This appendix contains a list of the conference papers published by the author which relate to the research presented in this thesis.

Davis, J.P., D.J. Walker, M. Townsend, and I.R. Young (2003), Spectral description of small scale wave formed rippled sediment beds, in *Proceedings of the International Conference on Coastal Sediments 2003 CD-ROM*, World Scientific Publishing Corp. and East Meets West Productions, Corpus Christi, Texas, USA.

Davis, J.P., D.J. Walker, M. Townsend, and I.R. Young (2001), The environmental significance of an intertidal sand shoal Adelaide South Australia, *Coasts & Ports Australasian Conference 2001, September 25–28*, Gold Coast, Australia, 20–25.

Townsend, M., J.P. Davis, D.J. Walker, and I.R. Young (2003), Wave dissipation over a sandy sea-bed, *Coasts & Ports Australasian Conference 2003, September 9–12*, Auckland, New Zealand, paper no. 153.

Walker, D., J.P. Davis, M. Townsend, and I.R. Young (2003), Observations of the growth of wave-induced ripples using a spectral approach, *Proceedings of 3rd IAHR Symposium on River, Coastal and Estuarine Morphodynamics, September 1–5*, Barcelona, Spain, 341–351.

Appendix B

Published Journal Paper

This Appendix presents a copy of a paper published in the Journal of Geophysical Research – Oceans which contains part of the research presented in this thesis. The citation details of this paper are:

Davis, J.P., D.J. Walker, M. Townsend, and I.R. Young (2004), Wave-formed sediment ripples: transient analysis of ripple spectral development, *Journal of Geophysical Research, 109*, C07020, doi:10.1029/2004JC002307.

NOTE: This publication is included on pp. 172-188 in the print copy of the thesis. It is also available online to authorised users at:

http://dx.doi.org/10.1029/2004JC002307

Appendix C

Wave Reflection Tests

This Appendix outlines the wave reflection tests that were undertaken to determine the efficiency of the wave dissipation beach installed in the wave flume.

C.1 INTRODUCTION

The dissipation beach was installed across the end of the flume to reduce wave reflections. It was constructed using a smooth 5 m wooden ramp at a slope of 1 in 10 to which a series of vertical mesh sections and a coarse rock bed were added to aid in wave dissipation through turbulent loss. The wave dissipation beach is shown in Plates C.1, C.2 and C.3.

The energy dissipation system consisted of three sections (refer to Plates C.1, C.2 and C.3). The first section consisted of a series of near vertical mesh sections through which the waves pass unbroken. As the waves passed through the 10 mm steel mesh they were dissipated due to an increase in turbulence over the total depth of the wave. The second section consisted of a series of four flexible plastic mesh sections which were designed to move under the oscillatory action of the waves. This section dissipated waves through turbulent loss and the transfer of mechanical energy to the mesh. The third section of the dissipation beach, which was located on the top section with a shallow water depth, was a rock bed. Waves broke onto this bed which effectively dissipated the kinetic energy of the wash. Holes were drilled into the beach above the rock bed so that any wash still present would fall through the beach and be able to return to the top of the tank via the 100 mm

Plate C.1 Wave dissipation beach from the front.

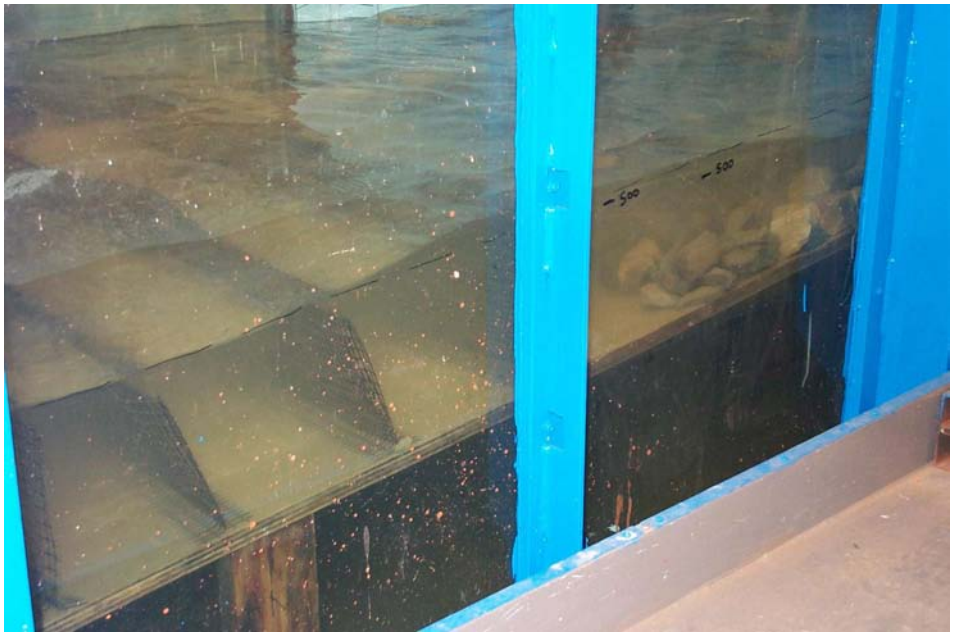

Plate C.2 Wave dissipation beach from the side.

Plate C.3 Wave dissipation beach from the back.

diameter pipe installed under the sand bed (refer to Section 3.1.2).

C.2 Experimental Procedure

To determine the wave reflection coefficient of the dissipation beach a two-dimensional wave spectra was calculated using the Maximum Likelihood Method (MLM) [*Young*, 1994]. This method requires that an array of wave gauges be setup with known polar (angles and distances) geometry. The MLM attempts to determine the directional spectrum which has the maximum likelihood of conforming to the limited number of cross-spectral estimates. The energy from a given angle is evaluated by minimising the influence from all other components. Minimisation is achieved through the use of a Lagrange multiplier [see *Young*, 1994, for further details]. A MATLAB function was provided by Prof. Ian Young to enable the calculation of the directional spectra from an array of wave gauges.

The array dimensions were designed so that the greatest directional resolution would be along the flume in the direction of both the incident and reflected wave energies. Incident wave energy is the energy due to waves generated by the wave paddle while reflected

wave energy is the wave energy being reflected from the wave dissipation beach. Plate C.4 shows the probe setup for the reflection tests. All probes were located on the centreline of the flume with a probe spacing in the direction of wave travel (from left to right) of 100 mm which is much less than the peak wavelength of the waves (refer to Table C.1). The array was located 14.8 m from the wave paddle (9.7 m from the start of the sand bed) and 10.5 m from the dissipation beach (at the end of the sand bed).

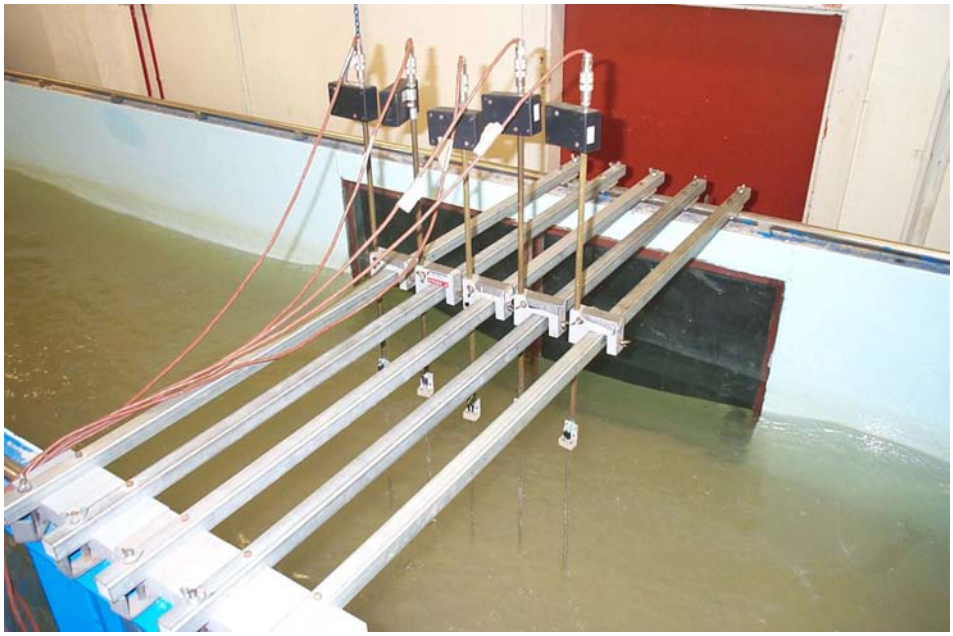

Plate C.4 The setup of the directional array for the wave reflection tests.

Figure C.1 shows a typical two-dimensional wave spectrum, that was measured via the array of probes and calculated using the MLM algorithm. The direction waves travel away from the wave paddle was defined as zero. As would be expected, Figure C.1 shows that most of the spectral energy is travelling away from the paddle with only a very small level of energy moving back along the flume towards the paddle.

Once the two-dimensional wave spectrum had been estimated a ratio was calculated to determine the reflection coefficient as a function of the wave frequency. The incident wave spectrum was defined as the frequency spectrum from the zero direction while the reflected spectrum was defined as the spectrum travelling from a direction of 180 degrees.

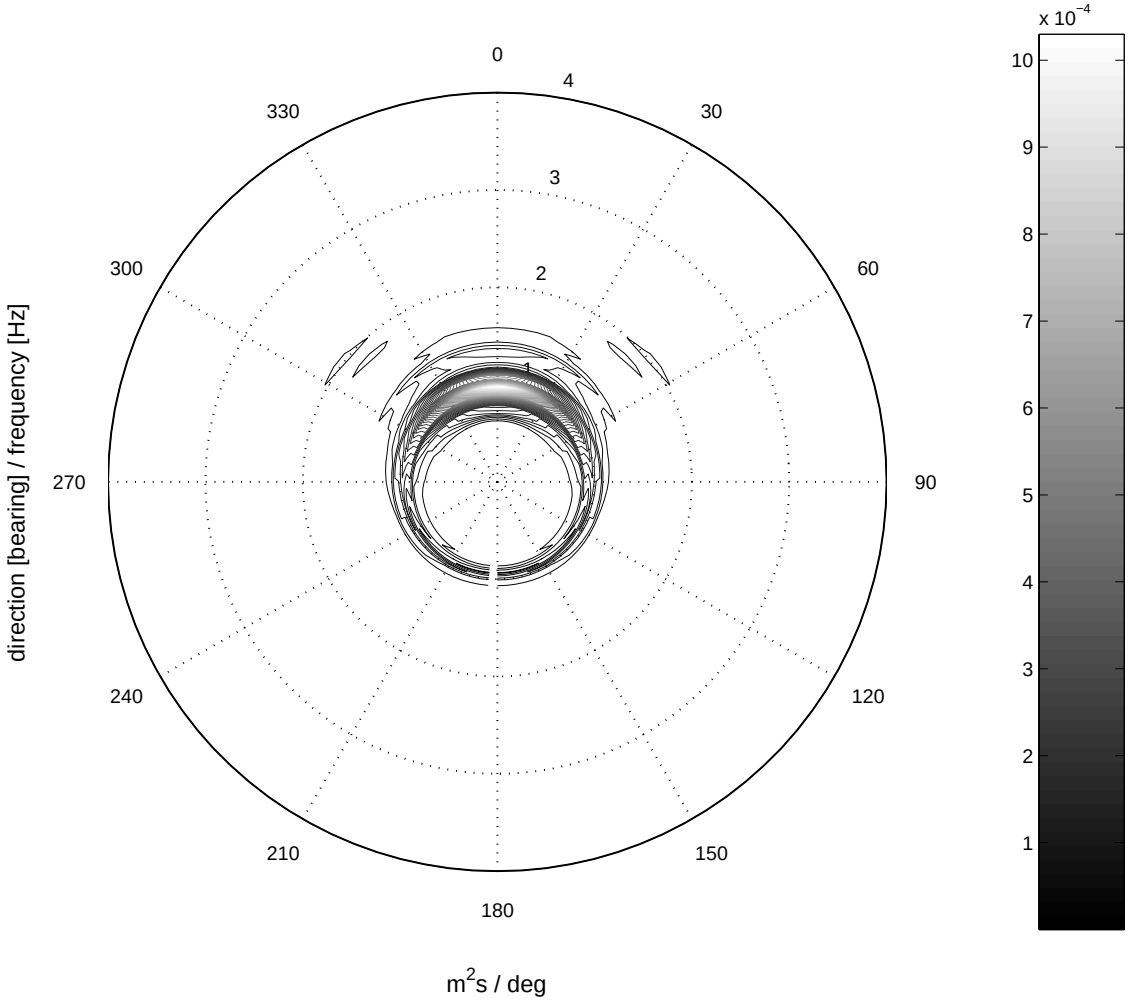

Figure C.1 A two-dimensional surface wave spectrum measured from the wave array.

This ratio is given as:

$$\Phi_r(f) = \frac{S_I(f)}{S_R(f)} \tag{C.1}$$

where Φ_r is the wave reflection coefficient; S_I is the incident wave energy spectrum (m^2/Hz); S_R is the reflected wave energy spectrum (m^2/Hz) and f is the surface wave frequency (Hz).

Table C.1 The wave reflection tests undertaken to test the efficiency of the dissipation beach.

Test ID	Wave type	$f_p(f)$ Hz	$H_s(H)$ m	$L_p(L)$ m	Test Time minutes
R01	irregular	1.0	0.087	1.373	21.6
R02	irregular	0.8	0.082	1.867	21.6
R03	irregular	1.2	0.072	1.023	21.6
R04	regular	1.0	0.113	1.373	20.0
R05	regular	0.8	0.072	1.867	20.0
R06	regular	1.2	0.110	1.023	20.0

C.3 Results and Discussion

This section presents the results of the reflection tests. Six wave reflection tests were undertaken using the setup shown in Plate C.4. Table C.1 list the tests undertaken. The test used to produce the two-dimensional spectrum shown in Figure C.1 is listed in Table C.1 as Test R03. Six tests were undertaken three with irregular waves and three with regular waves. The irregular waves conformed to a standard JONSWAP spectrum ($\gamma = 3.3$). The depth of water in all tests was 300 mm and the sampling frequency was 10 Hz. In Table C.1 f_p is the peak wave frequency (Hz), H_s is the significant wave height (m) and L_p is the wavelength corresponding to f_p (m). The terms shown in brackets are the regular wave equivalents. The test time relates to the period of time over which the waves were sampled.

Figures C.2, C.3 and C.4 show the reflection coefficient for the irregular wave tests of R01, R02 and R03 shown in Table C.1. There is very little energy being reflected from the wave dissipation beach in any of these tests. Reflected spectral energy for the frequencies near the peak frequency is less than 10% of the incident wave spectral energy. Away from the peak frequency there is a substantial percentage of energy being reflected, however, the value of the spectral energy across these frequencies is very small. From the irregular wave tests presented in Figures C.2, C.3 and C.4 there is less than 10% of wave energy being reflected across the frequency range of the generated surface wave spectrum.

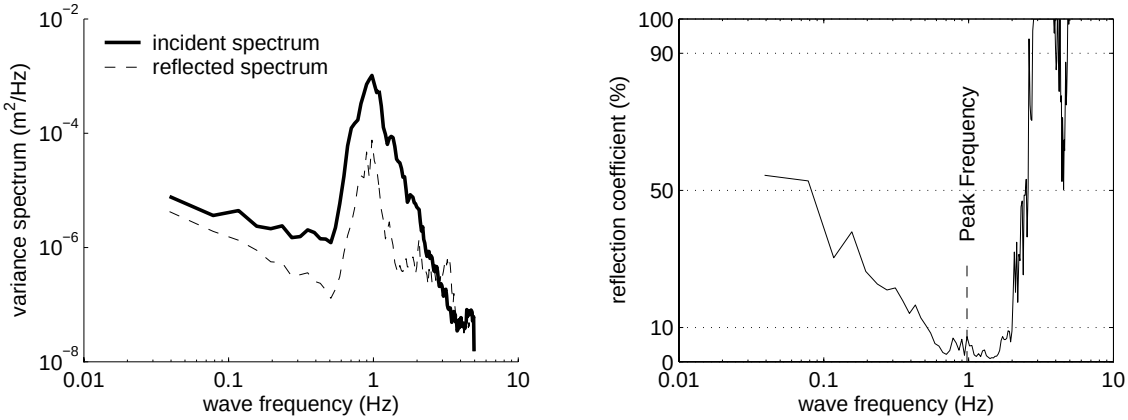

Figure C.2 Results of the wave reflection tests R01.

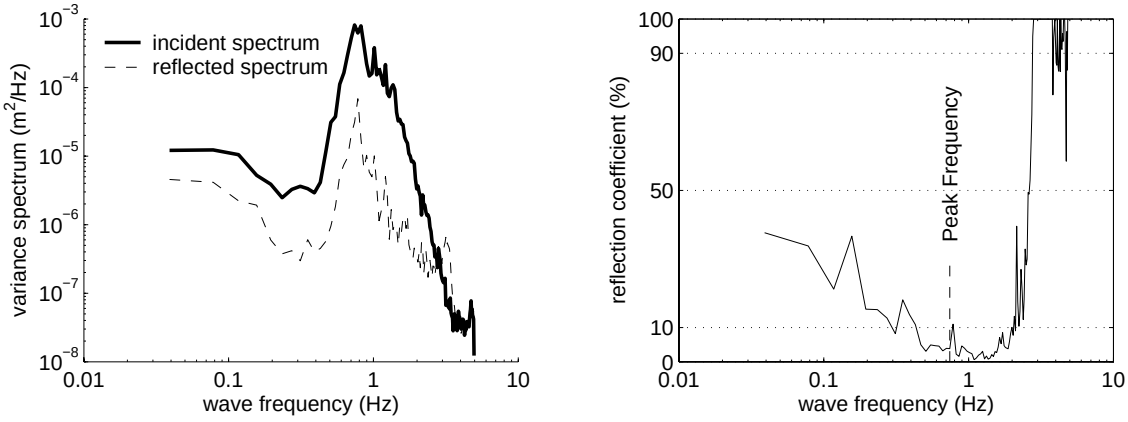

Figure C.3 Results of the wave reflection tests R02.

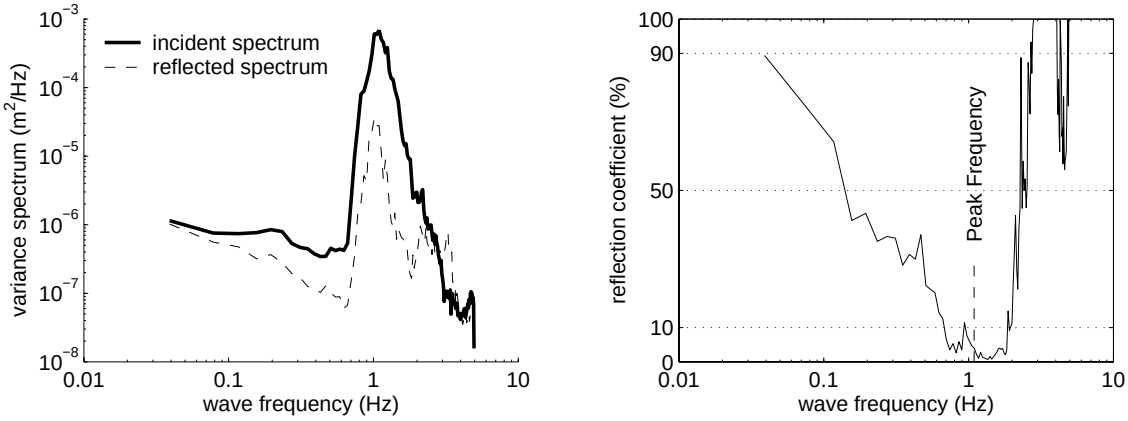

Figure C.4 Results of the wave reflection tests R03.

Undertaking a MLM reflection analysis on regular waves is slightly incorrect as it is a spectral method. It is impossible to produce perfect regular waves in the flume as all waves generated will not be exactly the same and their shape will be effected by the water depth. Hence, the waves generated will show some spectral attributes such as a slight range about some peak frequency value and a number of harmonics due to their shallow water cnoidal shape.

Figures C.5, C.6 and C.7 show the reflection coefficient for the regular wave tests of R04, R05 and R06 shown in Table C.1. As with the irregular waves there is very little energy being reflected from the wave dissipation beach in any of these tests. Reflected wave energy for the frequencies near the peak frequency is less than 10% of the incident wave spectral energy. There is a number of harmonics present within the spectra for the regular wave tests. As discussed above, these harmonics are due to the very cnoidal shape that regular waves exhibit in the shallow water. These harmonics were not present within the irregular wave spectra. As with the irregular reflection tests there is a substantial percentage of energy being reflected at those frequencies which lie outside the peak frequency range, however the value of the spectral energy across these frequencies is very small. Interestingly when a harmonic peak extends above approximately $1 \times 10^{-4}\ m^2/Hz$ there is a corresponding drop in the reflection coefficient to below 10%. From the data presented in Figures C.5, C.6 and C.7 there is less than 10% of wave energy being reflected by the regular waves.

C.4 SUMMARY AND CONCLUSION

A series of wave reflection tests were undertaken to determine the efficiency of the wave dissipation beach installed across the end of the wave flume. It is the conclusion of the wave reflection study that the wave dissipation beach works very well over the range of wave frequencies investigated. The dissipation beach is highly efficient at dissipating wave energy with less than 10% of the incident wave energy being reflected back along the wave flume.

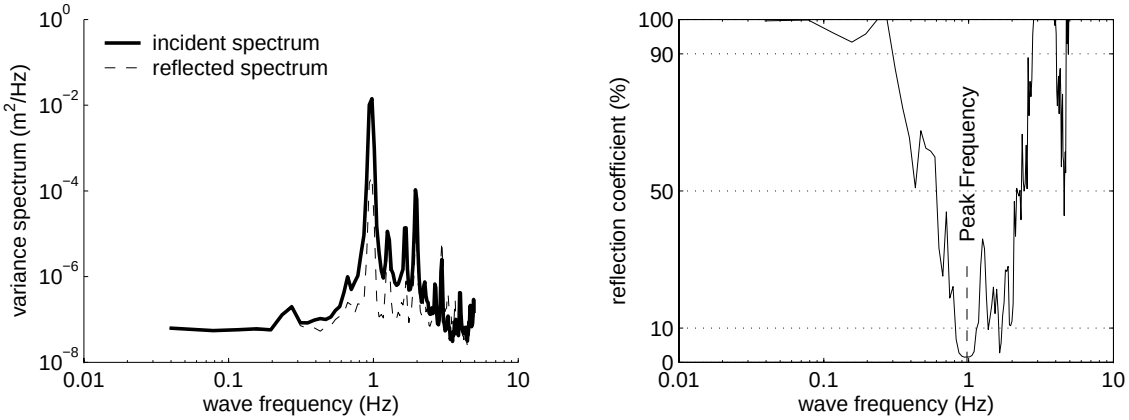

Figure C.5 Results of the wave reflection tests R04.

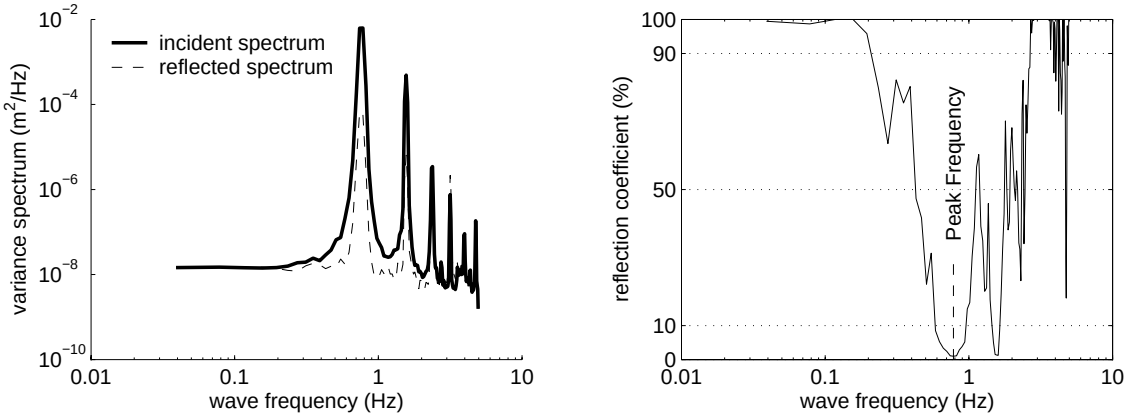

Figure C.6 Results of the wave reflection tests R05.

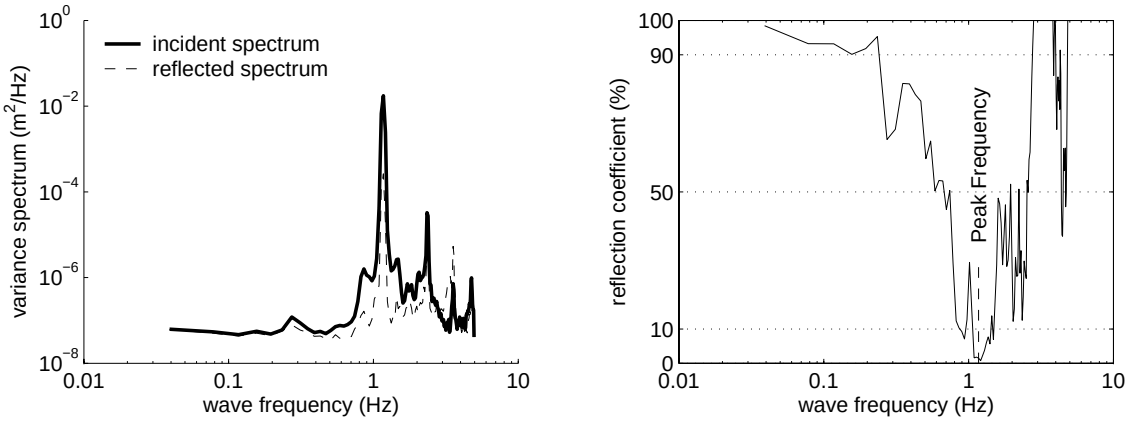

Figure C.7 Results of the wave reflection tests R06.

Appendix D

Wave Measurement Probes

This appendix outlines the calibration procedure and the experimental tests undertaken to determine the accuracy of the wave measurement probes used by this study. The calibration procedure summarised in this appendix was undertaken before each experimental test, while the accuracy tests were undertaken in the initial startup phase of the experimental component of this body of research.

To measure the time series of the surface waves, a set of five surface penetrating resistance wave probes were used (refer to Plate C.4, page 192). The probes had a measurement range of 250 mm and output voltages in the range of ± 5 V. The probes were linked to a data logging computer via an analog-to-digital board. The time series data of the water surface elevation was written to the computer screen and to file via data acquisition software written using the *Visual Designer*^{TM} suite (copyright 1993-1997 Intelligent Instrumentation). Before each test the probes were calibrated using 5 data points over a range of 250 mm, checked for stability and zeroed. Due to some high frequency electrical noise being evident within the time signal of the preliminary set-up tests, a high frequency single pole resistance-capacitance filter was applied to the output of each probe. This filter removed signal noise above a frequency of 60 Hz and consisted of a capacitor of value 0.22 mF and a resistor of 12 $k\Omega$. The wave probes were sampling at a frequency of 8 Hz to reduce aliasing effects.

D.1 WAVE PROBE CALIBRATION PROCEDURE

Before any of the experimental work was started, a series of 50 mm increments were engraved onto the probes' shafts and software using the *Visual Designer*^{TM} suite (copyright 1993-1997 Intelligent Instrumentation) was written to display the raw probe voltages. This made calibrating the probes more consistent and convenient.

Prior to each experimental test the wave probes were calibrated according to the following procedure:

1. The water level in the wave flume was set to the desired depth and allowed to settle;
2. All probes were moved up till they were at the bottom 50 mm calibration increment and the voltage output recorded;
3. The probes were then moved down to the next 50 mm increment and once again the output voltage was recorded;
4. The previous step was repeated until the probes had been moved through their 250 mm measurement range;
5. The voltages and heights were plotted and a straight line fitted to the output data recorded from each probe;
6. The slope determined from the straight line fit for each probe was recorded and entered into the data logging software;
7. The probes were moved until they showed a zero output (i.e. a zero voltage output);
8. The probes were left recording the flat water surface for 10 minutes to ensure that the output was stable;

Figure D.1 presents typical results for the calibration of the wave measurement probes. The magnitude of the linear correlation coefficient (R^2) shown in these figures was a typical observed value. The slope and offset of the probes calibration were affected by the temperature of the water and hence were not constant during the 12 month experimental

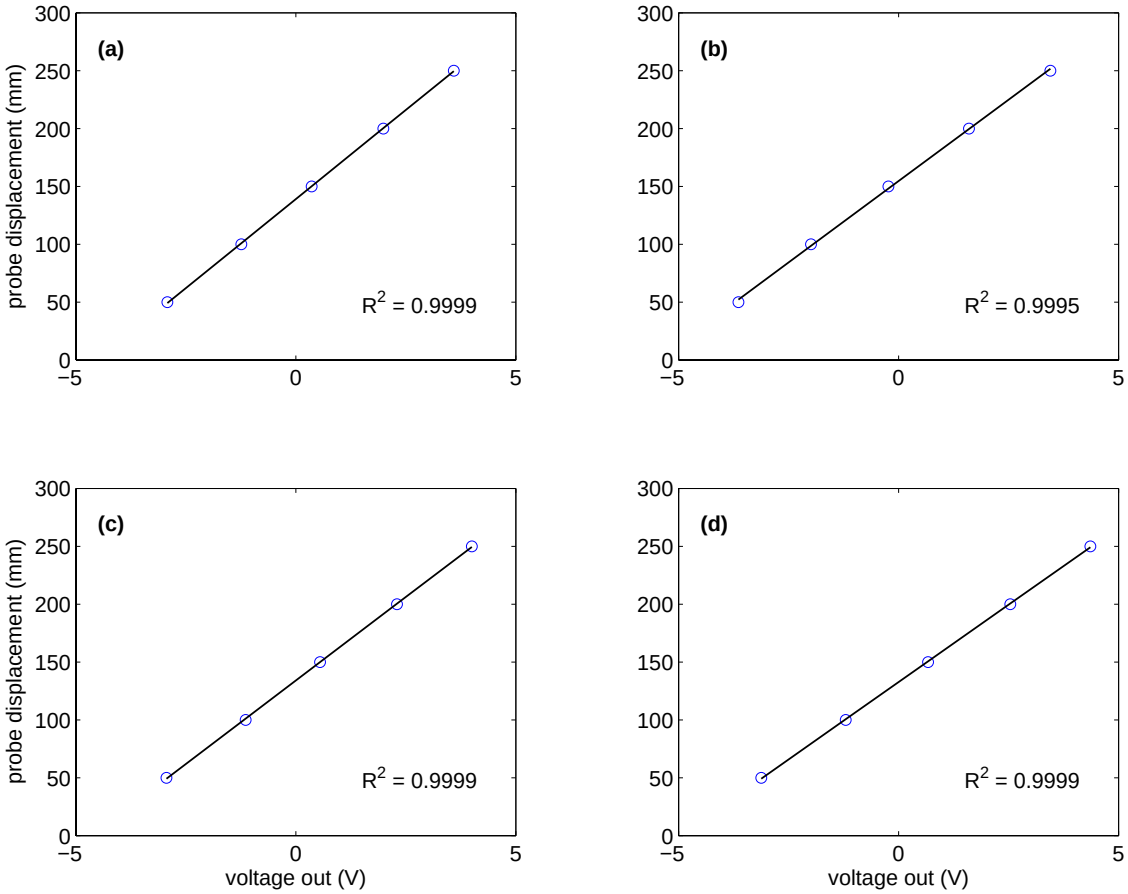

Figure D.1 A typical result for the calibration of the wave measurement probes where subplots (a) to (d) represent probes #0 to #3. Please note probe #4 is not shown.

phase. This problem was overcome by ensuring that the probes were calibrated prior to each test being undertaken.

D.2 Wave Probe Accuracy Tests

Initially this study was going to attempt to use the wave probes to determine the change in wave dissipation rates along the flume due to the formation of ripples. Hence, the work presented in this section was undertaken on the wave probes to try and determine their measurement accuracy. However, the change in the water surface due to ripple formation and subsequent wave dissipation was not included in this thesis, but might be reanalysed and published in the future.

A series of runs were undertaken to test the accuracy of the wave probes. This was done by testing the probes against each other in a series of specific experimental tests. All tests presented below all used an irregular surface wave condition with a standard ($\gamma = 3.3$) JONSWAP spectral shape, a peak frequency of 1 Hz and a significant wave height of 0.1 m.

D.2.1 Probe Test #1

Probe test #1 was undertaken to determine how well the probes recorded waves compared to each other across the flume. For this test the probes were placed at a distance of 7 m from the wave paddle across the flume in the configuration shown in Figure D.2. The test time was 25 minutes and 30 seconds with the surface wave time series being sampled at 8 Hz which gave a spectral estimate with 190 degrees of freedom using a spectral window of 128 data points.

Theoretically all the probes in this test should of given the same results, however, this was not the case. Figure D.3 shows the results recorded for each probe. As shown, Probe #1 gave the highest results while Probe #0 gave the lowest. There is a trend of decreasing significant wave height right to left across the wave flume. The average of the 4 probes is 0.103 m with a fluctuation of 0.015 m across the flume.

It is unclear from probe test #1 if there is a real variation in wave height across the flume or if it is inaccuracies of the wave probes that are showing up in the tests.

D.2.2 Probe Test #2

Probe test #2 was undertaken to determine how well the probes recorded waves compared to each other along the flume. For this test the probes were setup at a distance of 7 m from the wave paddle along the flume with the probes being positioned as close as possible to each other, as shown in Figure D.4. The test time was 25 minutes and 20 seconds with the surface wave time series being sampled at 8 Hz which gave a spectral estimate with 190 degrees of freedom using a spectral window of 128 data points.

The results of probe test #2 are presented in Figure D.5. Please note that only three

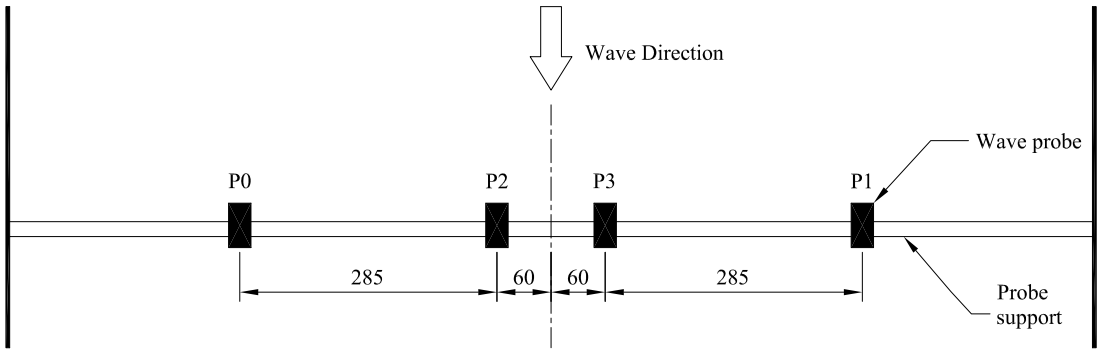

Figure D.2 Schematic showing the wave probe setup for probe test #1 (all dimensions shown are in mm).

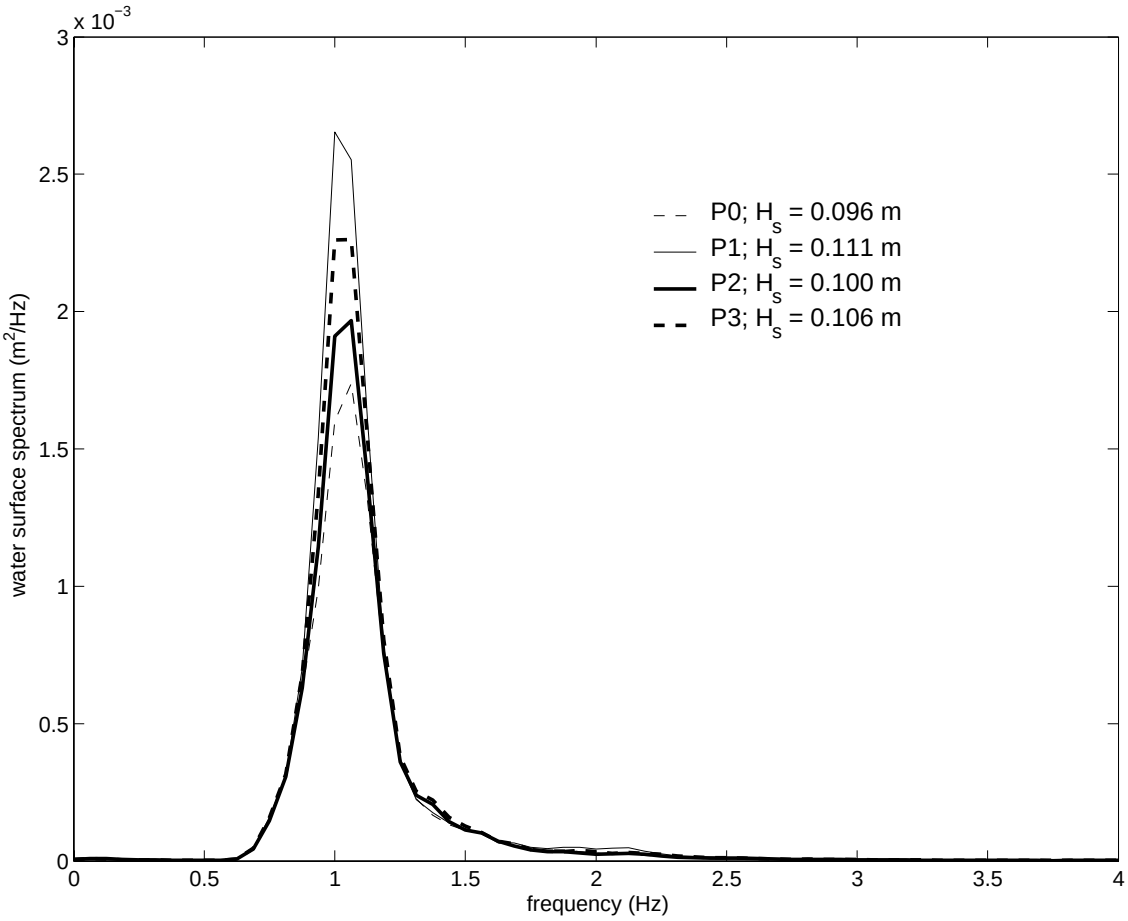

Figure D.3 Spectra measured from probe output for probe test #1.

probes were used for this particular test.

As can be seen in Figure D.5 the variation in significant wave height for test #2 is much smaller than for test #1. The average significant wave height for the three probes was 0.107 m with a fluctuation of 0.003 m.

The results of this test when viewed in respect to the results of probe test #1 above suggests that there is a pronounced fluctuation of significant wave height across the wave flume. In probe test #1 there was a substantial fluctuation in the output from the probes, however, this was not present in the results shown for probe test #2. This indicates that the observed fluctuation was due to a variation in the water level across the flume and not due to a fluctuation in the probes output.

D.2.3 Probe Test #3

To test the above result, that there was a fluctuation of significant wave height across the flume, a third test was established and run. For this test the waves were run continuously for 1 hour and 11 minutes while four sub-tests (a to d) were undertaken. Waves were run for a period of 5 minutes before the first test being recorded.

The test used four wave probes at locations across the flume similar to probe test #1. Probe tests #3a and #3b were recorded at a distance of 10 m from the wave paddle while tests #3c and #3d were run at a distance of 15 m from the wave paddle. The probe positions across the flume were reversed after approximately 15 minutes of recording. Each of the four sub-tests will be discussed in turn as part of this section.

Probe test #3a was setup across the flume, as shown in Figure D.6, some 10 m from the wave paddle. The run duration was 14 minutes and 23 seconds with the water surface sampled at 8 Hz, giving a spectral estimate with 110 degrees of freedom (spectral window of 128 data points).

The results of probe test #3a are shown in Figure D.7. Once again we see the trend of decreasing significant wave height as we move right to left across the wave flume. The average of all four probes is 0.104 m with a fluctuation of 0.009 m across the flume.

Probe test #3b was also located 10 m from the wave paddle, however, the probes

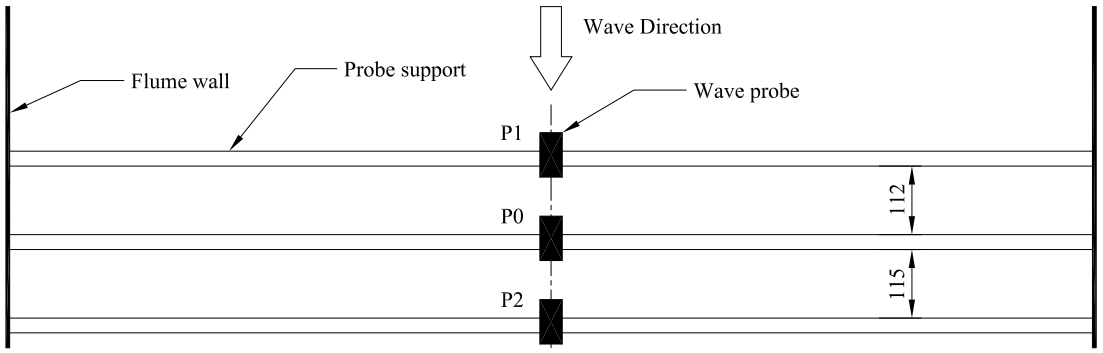

Figure D.4 Schematic showing the wave probe setup for probe test #2 (all dimensions shown are in mm).

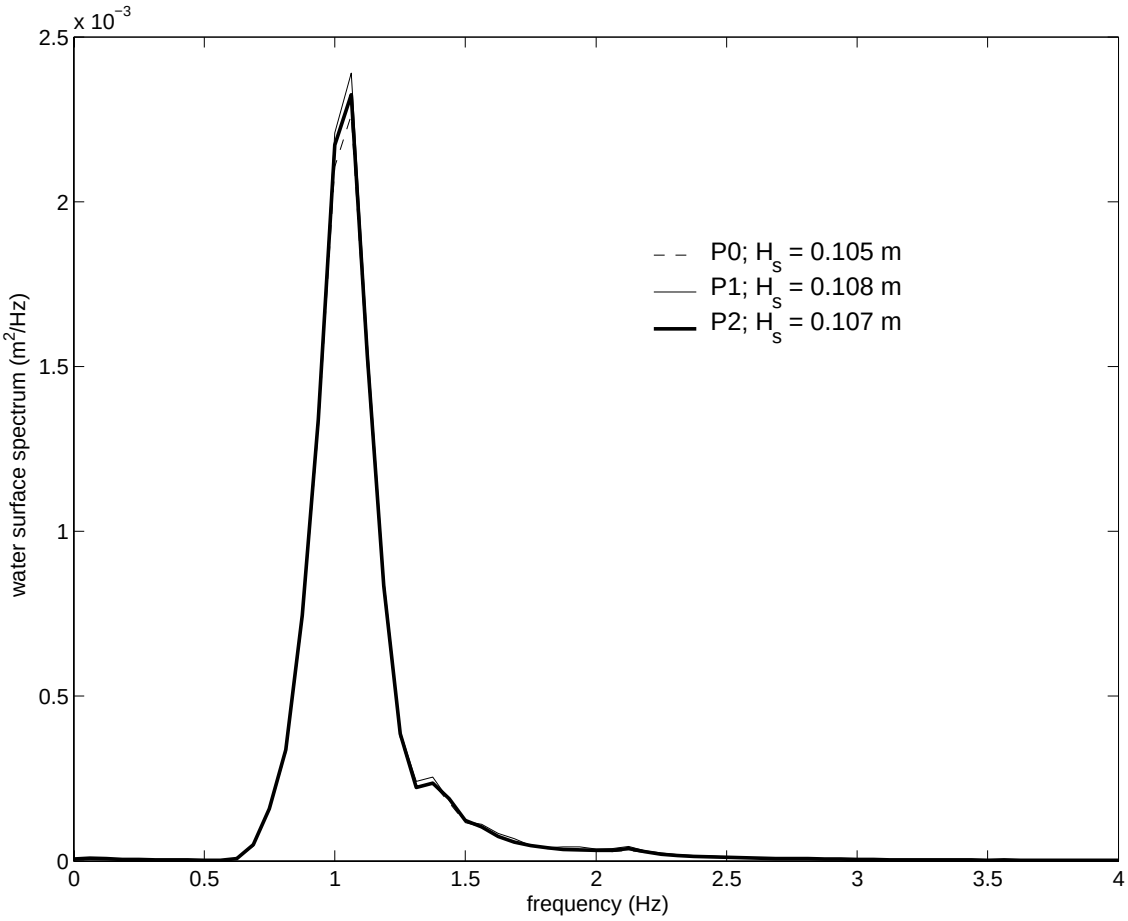

Figure D.5 Spectra measured from probe output for probe test #2.

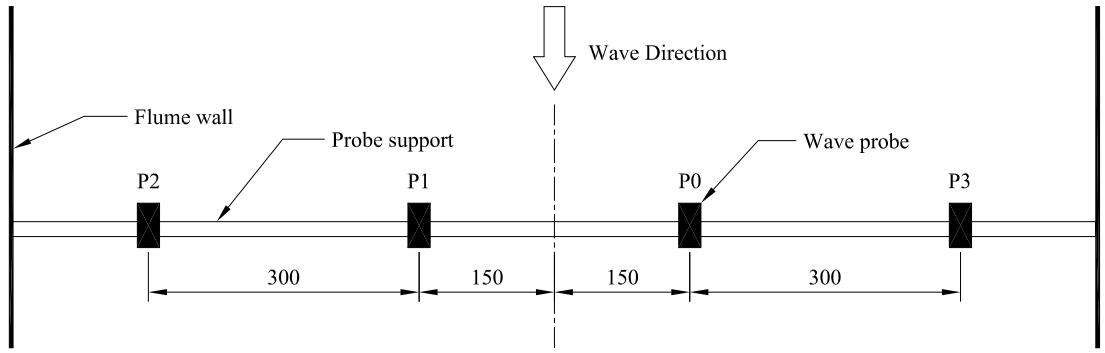

Figure D.6 Schematic showing the wave probe setup for probe test #3a and #3c (all dimensions shown are in mm).

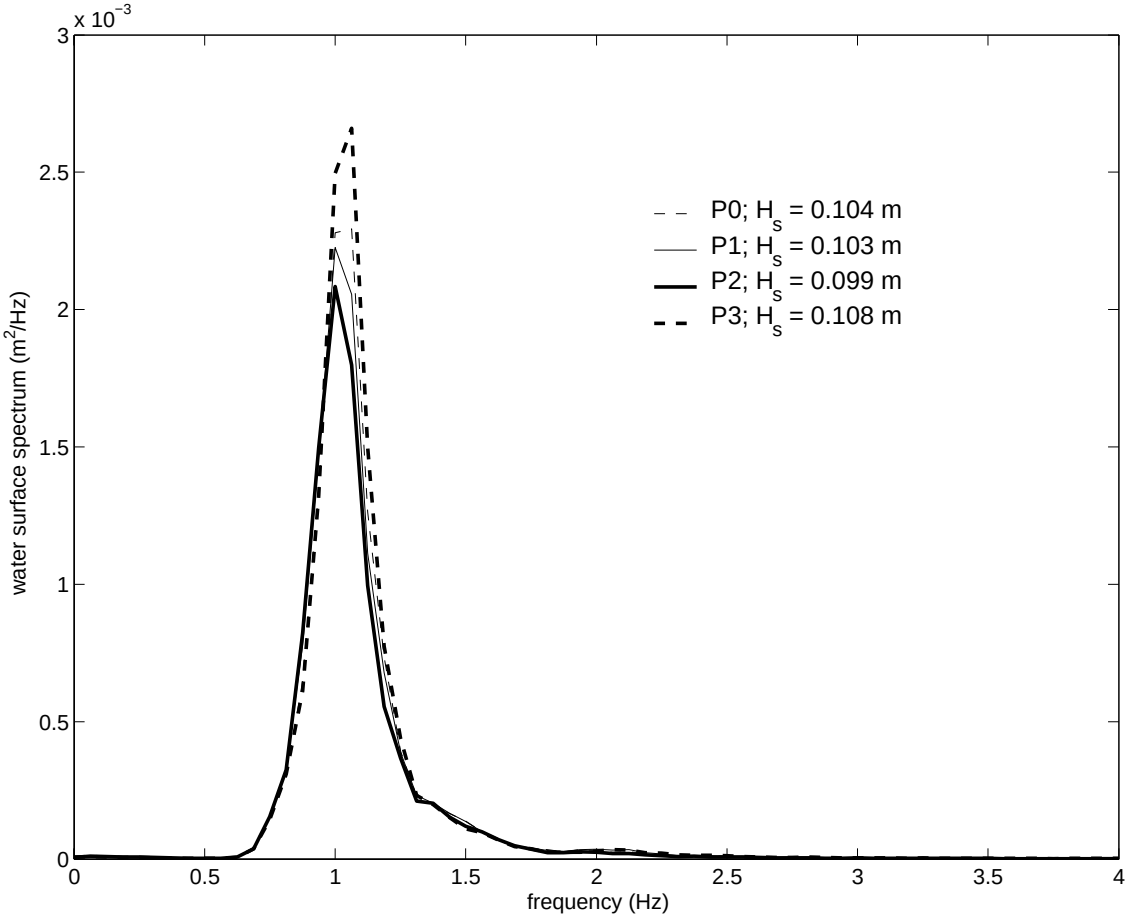

Figure D.7 Spectra measured from probe output for probe test #3a.

were reversed across the flume as shown in Figure D.8. The run duration was 14 minutes and 22 seconds with the water surface being sampled at 8 Hz, giving a spectral estimate with 110 degrees of freedom (spectral window of 128 data points).

The results of probe test #3b are presented in Figure D.9. Again we see the trend of decreasing significant wave height across the flume in Figure D.9, however this trend is smaller than that shown in Figure D.7. The average of all four probes is 0.101 m with a fluctuation of 0.005 m across the flume.

Probe test #3c was exactly the same as for probe test #3a, however, the probes were located at a distance of 15 m from the wave paddle. The wave probe set up across the flume is shown in Figure D.6. The run duration of probe test #3c was 14 minutes and 34 seconds with the water surface being sampled at 8 Hz, giving a spectral estimate with 110 degrees of freedom (spectral window of 128 data points). The results of this test are shown in Figure D.10.

The same trend as was shown at a distance of 10 m from the paddle (refer to Figure D.7), can also be seen at a distance of 15 m from the paddle (refer to Figure D.10). Again we see the decreasing significant wave height across the flume. The average of all four probes is 0.104 m with a larger fluctuation of 0.018 m across the flume.

Probe test #3d was exactly the same as for probe test #3b, except the probes were located at a distance of 15 m from the wave paddle, not 10 m. The wave probe set up across the flume is shown in Figure D.8. The run duration of probe test #3d was 14 minutes and 34 seconds with the water surface being sampled at 8 Hz, giving a spectral estimate with 110 degrees of freedom (spectral window of 128 data points). The results of this test are shown in Figure D.11.

The results once again show that there is a trend of decreasing significant wave height as we move from right to left across the flume. The average of all four probes, shown in Figure D.11 is 0.010 m with a fluctuation of 0.007 m across the flume.

The overall conclusion of probe test #3 is that there is a definite fluctuation of significant wave height as we move from the right to left across the flume. This fluctuation is not always constant so there may also be some slight inaccuracy in individual wave probes as

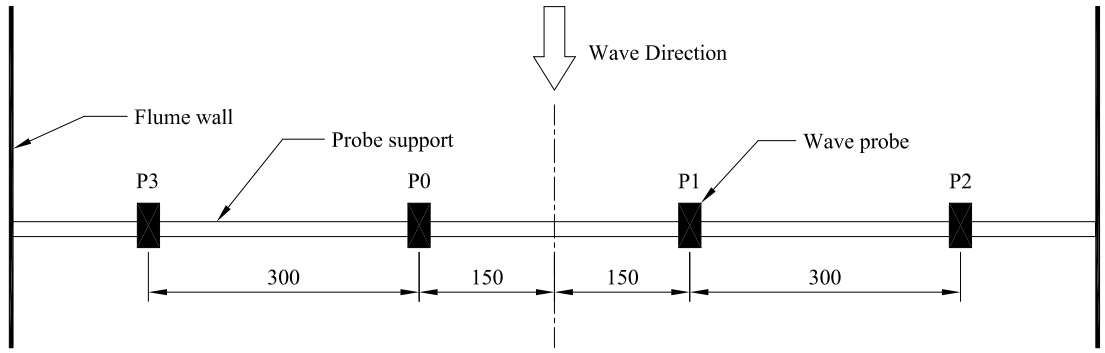

Figure D.8 Schematic showing the wave probe setup for probe test #3b and #3d (all dimensions shown are in mm).

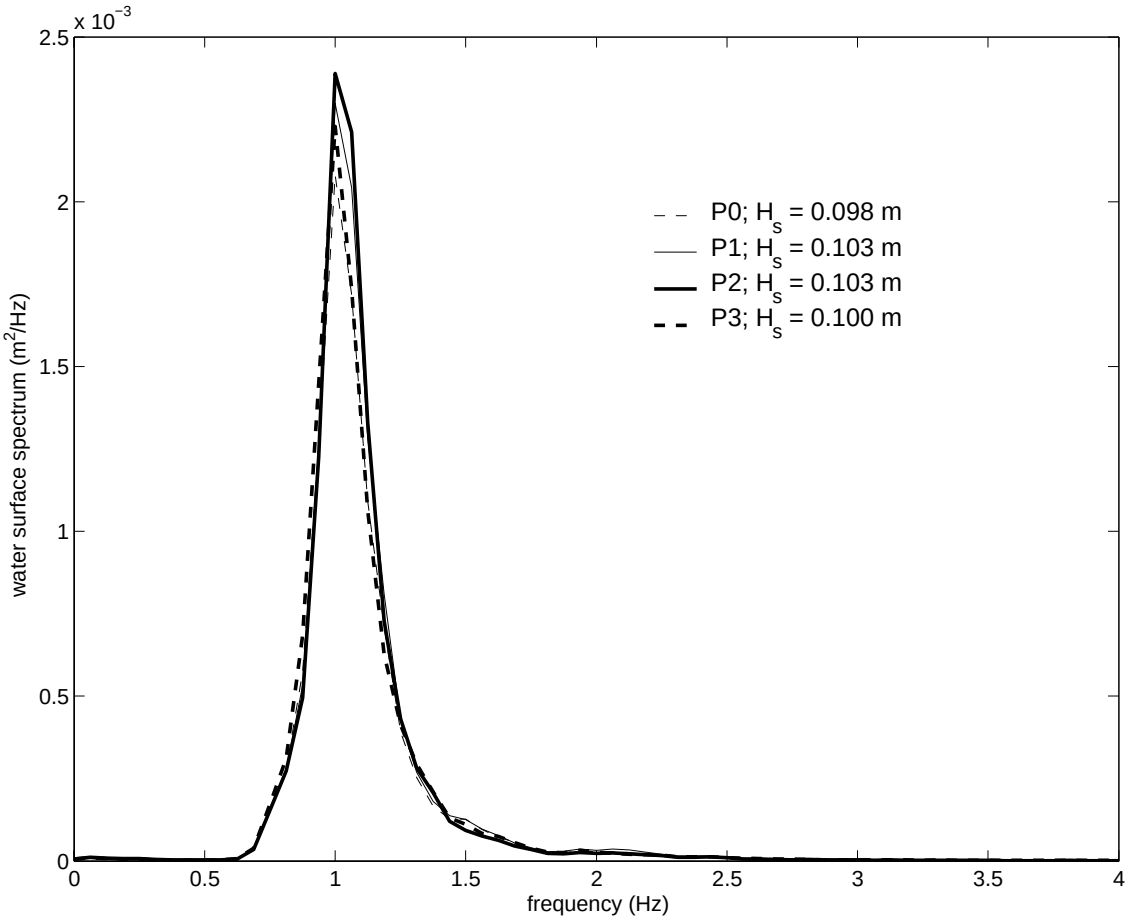

Figure D.9 Spectra measured from probe output for probe test three B.

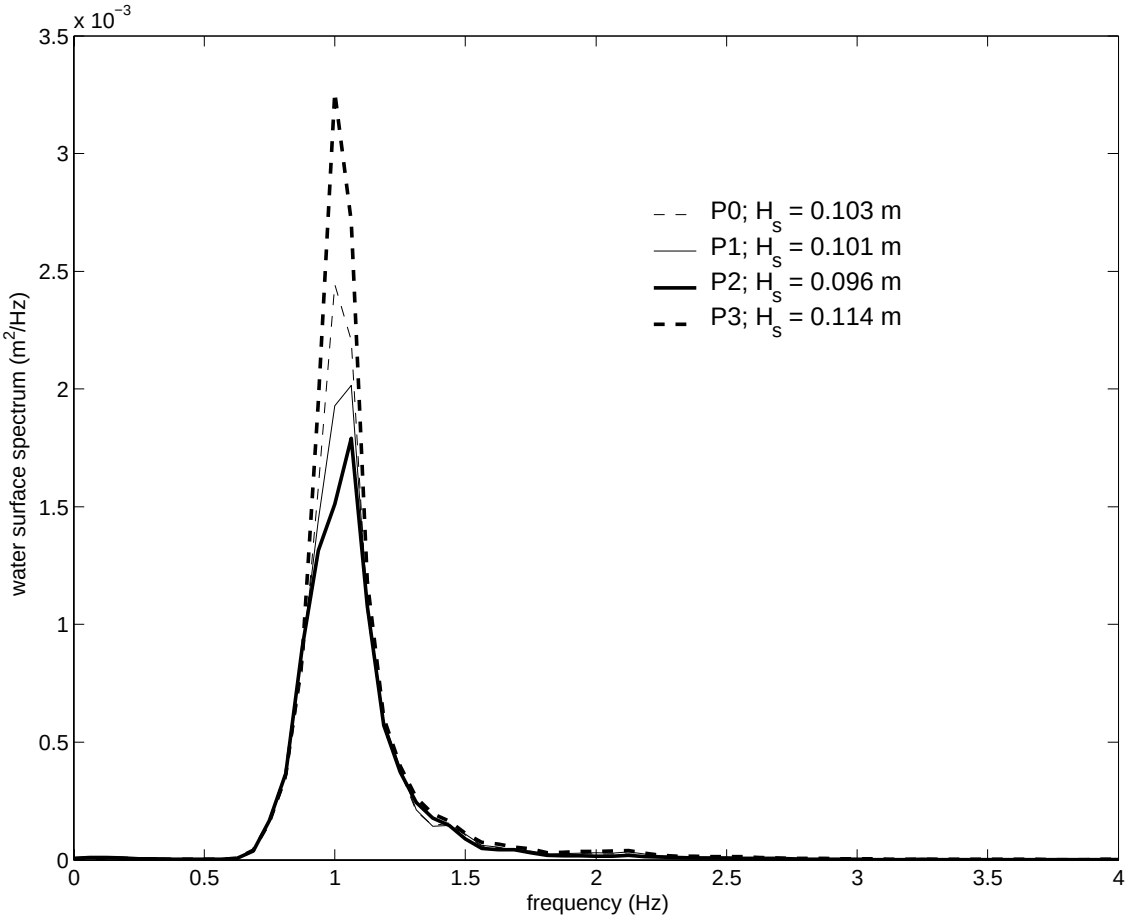

Figure D.10 Spectra measured from probe output for probe test three C.

well. However, the results suggests that the fluctuation of the water surface height across the flume is substantially larger than the measurement error of the individual probes.

D.3 SUMMARY AND CONCLUSION

This appendix outline the calibration procedure and a series of tests to determine the accuracy of the wave measurement probes.

The calibration procedure was presented in Section D.1. This procedure was undertaken prior to each experimental test being undertaken. The procedure worked very well and provided a consistent calibration method during the 12 month experimental period of this research project.

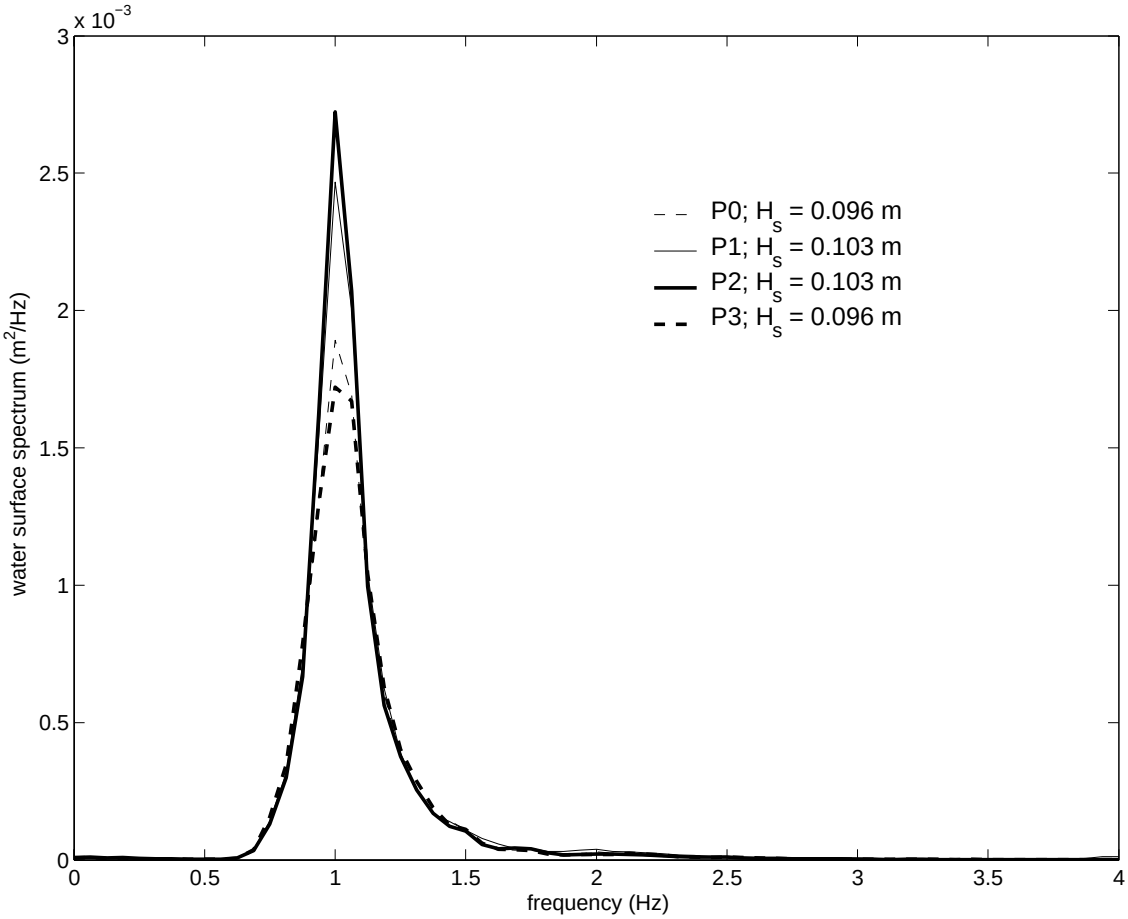

Figure D.11 Spectra measured from probe output for probe test three D.

The accuracy of the wave measurement probes was discussed in Section D.2. It was determined that the probes have a measurement error less than the fluctuation of the water surface across the flume which was in the order of 5 to 20 mm. These fluctuations were most probably due to the wave paddle being slightly out of alignment with the walls of the flume which caused slight wave reflections from the sides of the flume to be present in the wave spectrum. Appendix C discusses the test undertaken to determine the wave reflections in the flume. As shown in Figure C.1 (page 193), there is a substantial spread of energy present in the two-dimensional spectrum. This was not of major concern to the experiments undertaken as part of this research, but it does make using the water surface record to determine wave dissipation rates problematic. From probe test #2 it can be concluded that the measurement error of the individual probes is in the order of 0.003 m,

hence, only dissipations greater than 3 mm can be measured.

On the whole the use of the wave measurement probes allowed this study to measure the water surface time series with the required accuracy for the experimental tests undertaken.

Appendix E

Ripple Measurement System

This appendix presents extra details of the ripple measurement system (refer to Plate E.1) designed by the author and constructed by the technical staff in the School of Civil and Environmental Engineering, The University of Adelaide. Details will be presented as a series of drawings and photographs.

Plate E.1 The X-Y positional table of the ripple measurement system designed and developed by this study.

E.1 THE POSITIONAL TABLE

The X-Y positional table consists of two carriages mounted on an existing instrument trolley that was able to be moved along the wave flume (refer to Figures E.1 and E.2). The two carriages are called the primary and secondary carriage which relates to the direction they travel across the sand bed. As was outlined in Chapter 3 the axis along the flume in the direction of wave travel was defined as the primary axis while the secondary axis was defined as the axis across the flume normal to the direction of wave travel. Each carriage is driven by a 5 mm lead screw connected to a 1.8° step motor and mounted on stainless steel shafts and linear bearings. A 5 mm lead screw moves the nut 5 mm in the along shaft direction for every revolution.

Figures E.1 and E.2 show the plan and front views of the ripple measurement system. As can be seen in Figure E.2 the laser displacement sensor is encased in a clear water tight perspex tube and is located under the water surface. Figure E.3 presents a more detailed drawing of the secondary carriage, while Figure E.4 presents a detailed drawing of the primary carriage.

The plates shown in this appendix show a number of different views of the ripple measurement system.

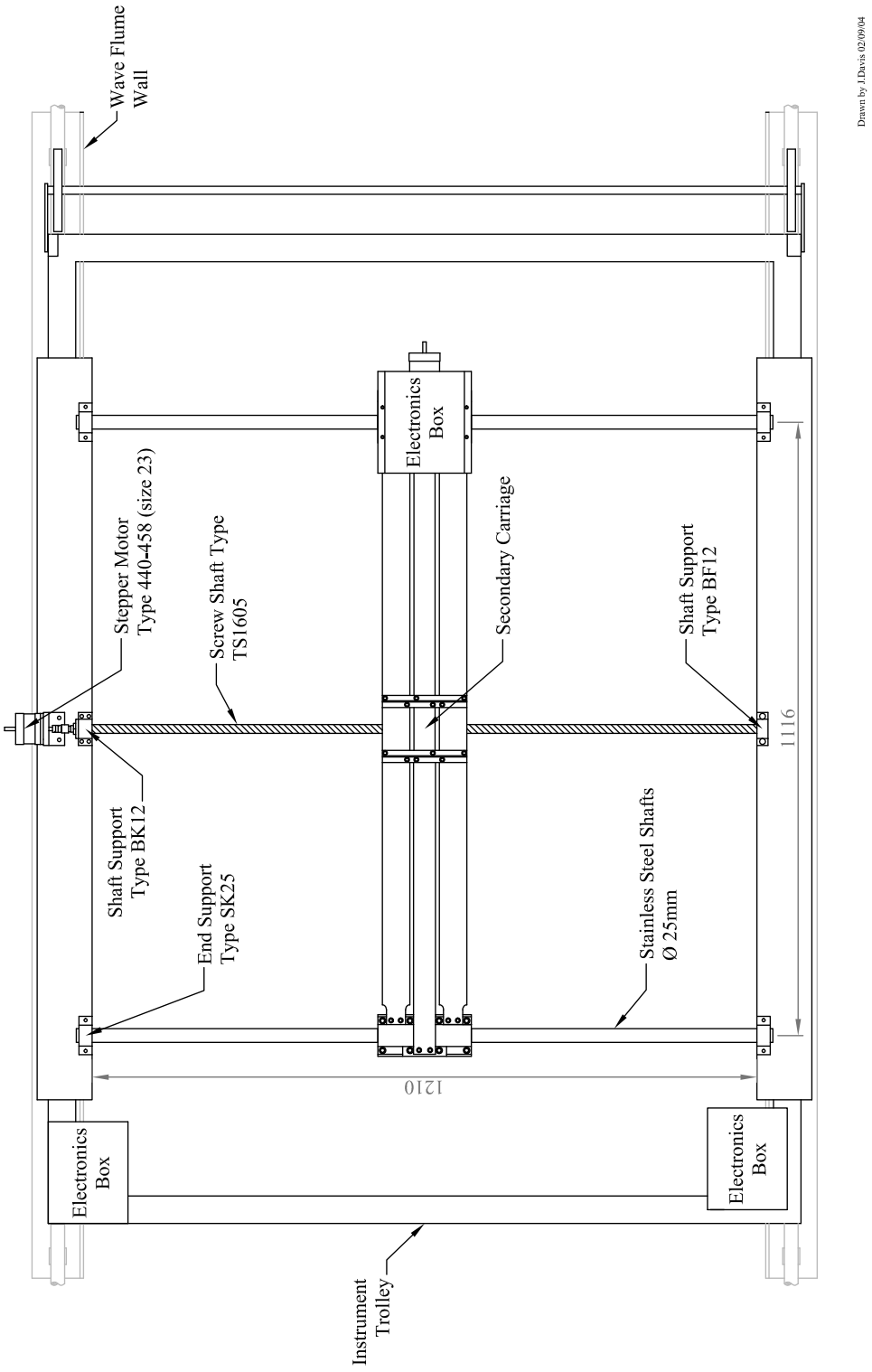

Figure E.1 The plan view of the ripple measurement system (all dimensions shown are in mm).

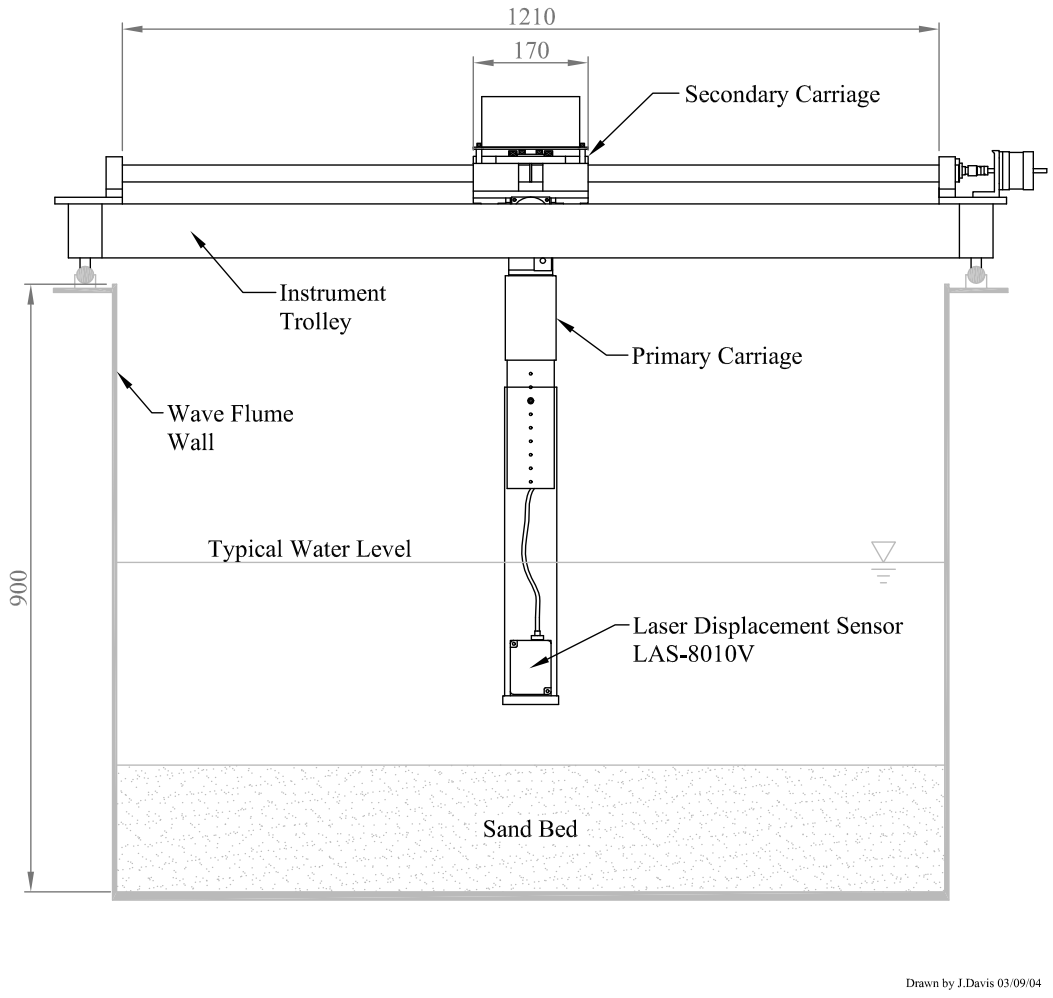

Figure E.2 The front view of the ripple measurement system (all dimensions shown are in mm).

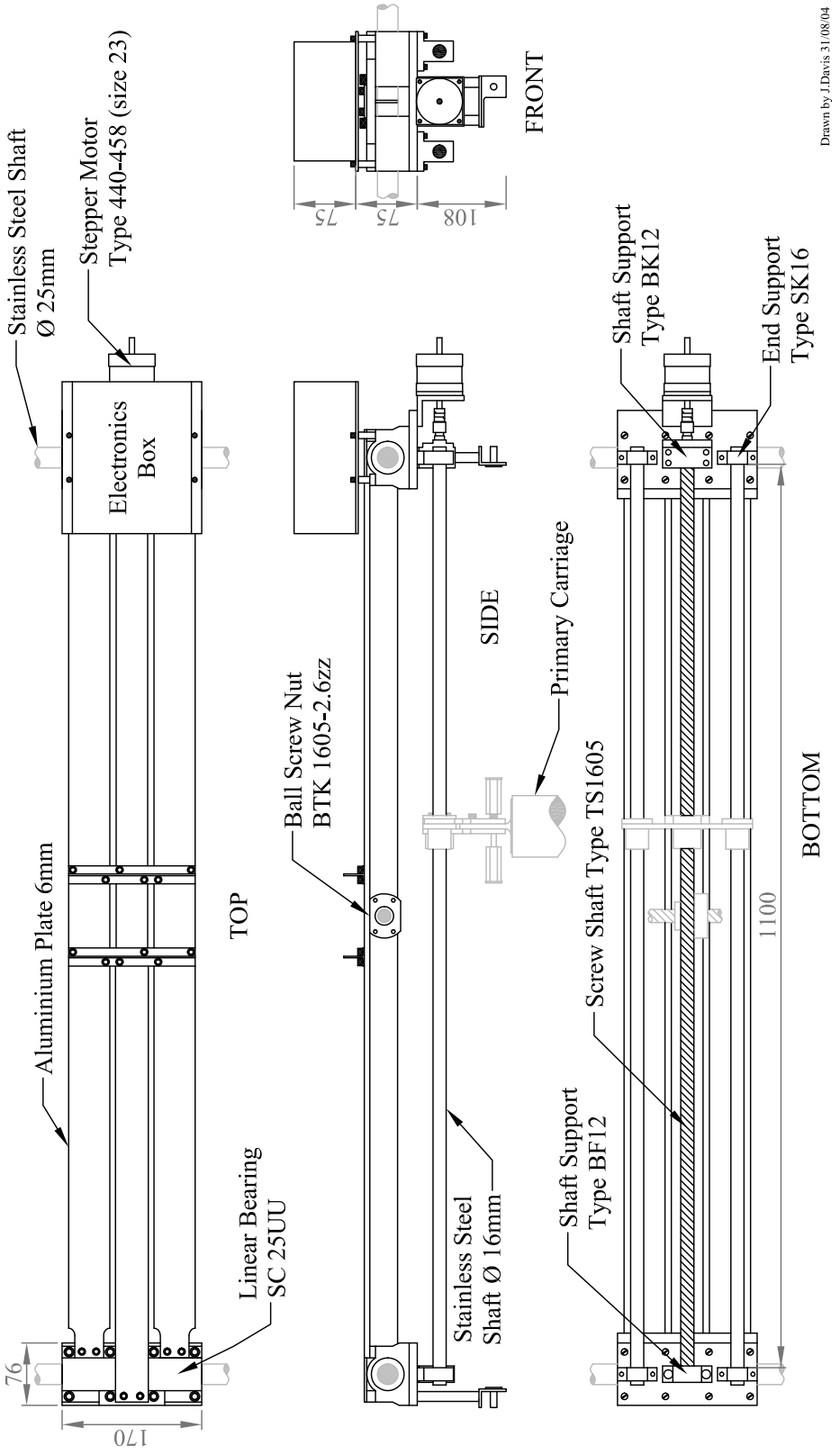

Figure E.3 The secondary carriage of the ripple measurement system (all dimensions shown are in mm).

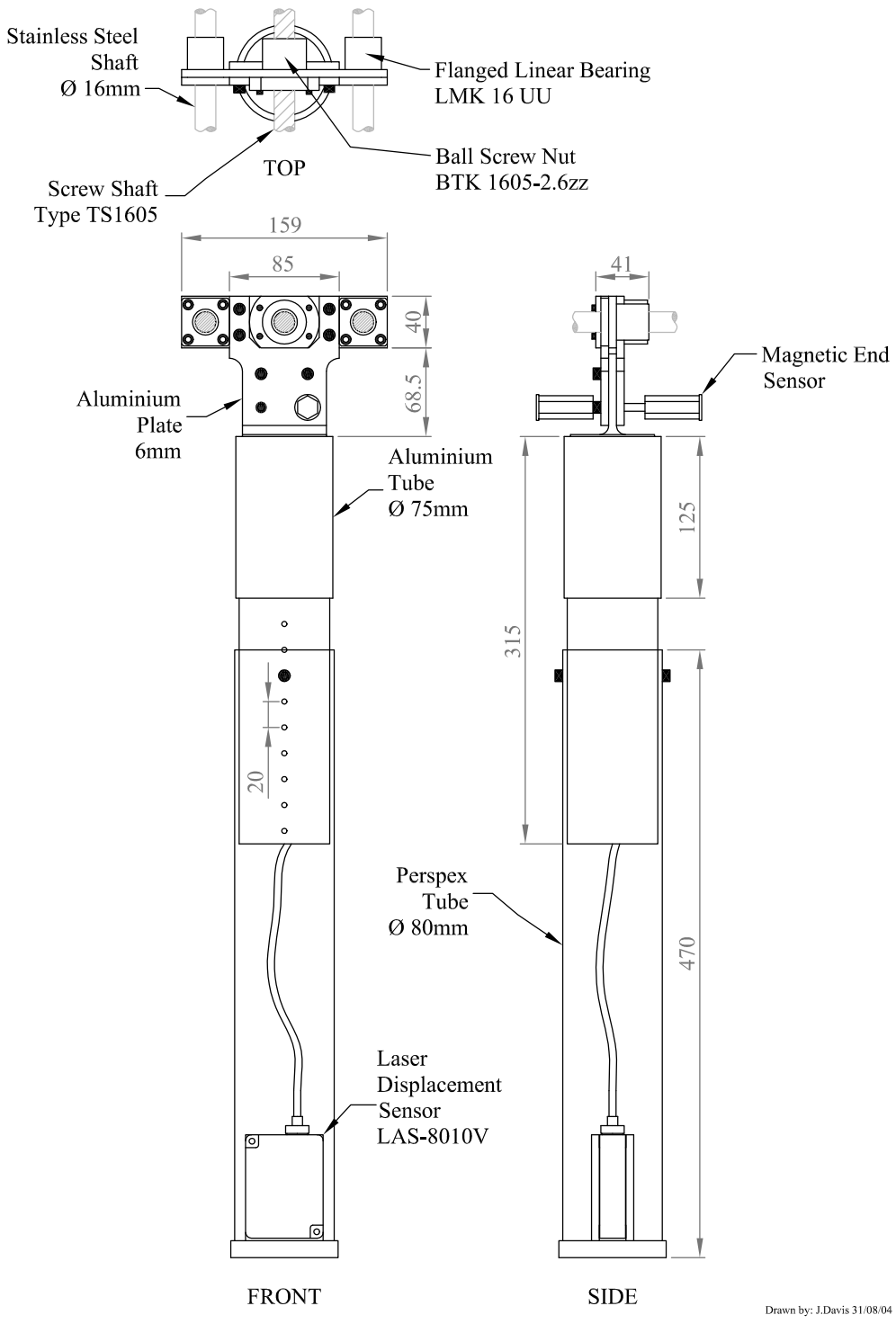

Figure E.4 The primary carriage of the ripple measurement system (all dimensions shown are in mm).

Plate E.2 The primary carriage of the ripple measurement system.

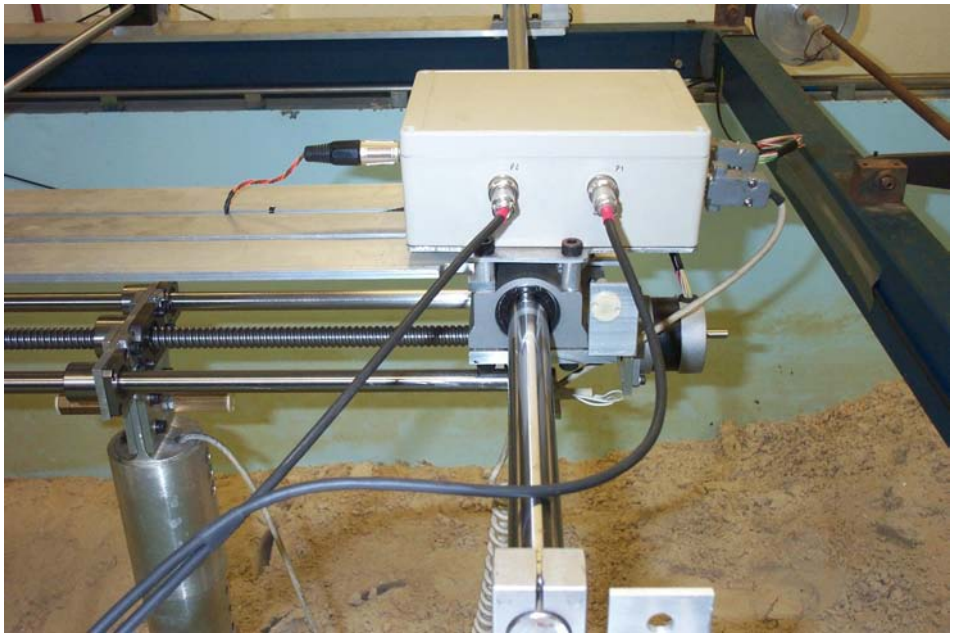

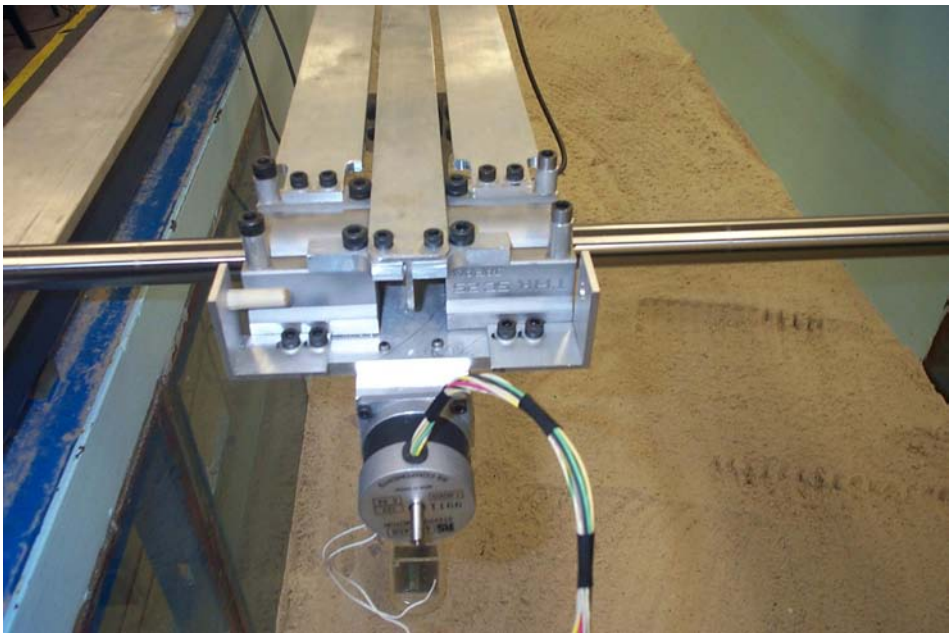

Plate E.3 Two views of the linear bearing support of the secondary carriage of the ripple measurement system.

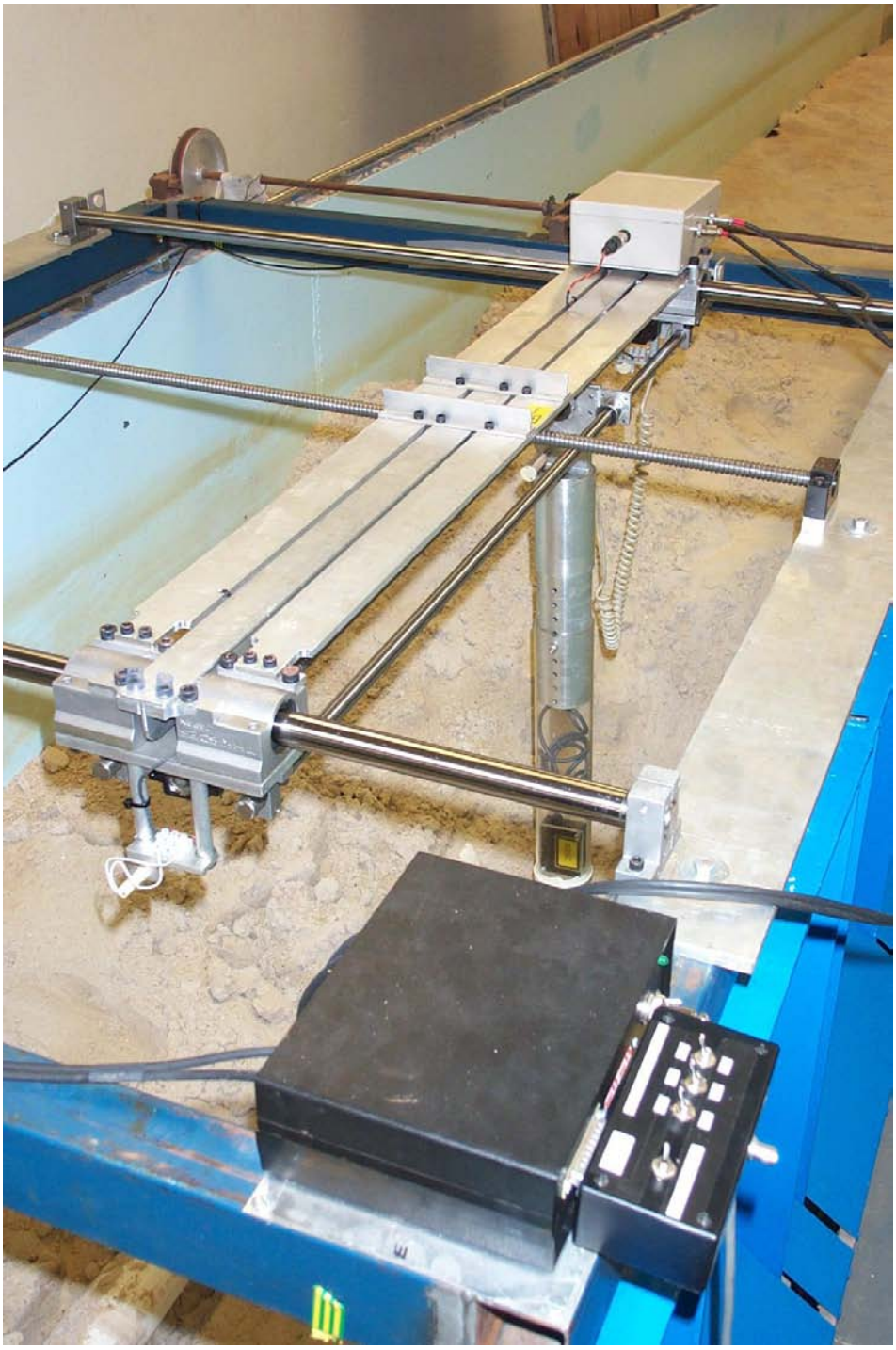

Plate E.4 The top view of the ripple measurement system.

Plate E.5 The top view of the ripple measurement system.

Plate E.6 The primary carriage of the ripple measurement system.